RSC Advances

ROYAL SOCIETY OF CHEMISTRY

www.rsc.org/advances

Cite this: DOI: 10.1039/c0xx00000x

www.rsc.org/xxxxxx

ARTICLE TYPE

Star-shaped POSS diblock copolymers and their self-assembled films

Aizhao Pan, Shao Yang, Ling He* and Xiang Zhao*

Received (in XXX, XXX) Xth XXXXXXXXX 200X, Accepted Xth XXXXXXXXX 200X
DOI: 10.1039/b000000x

Novel 16-arm star-shaped POSS-containing diblock copolymers are firstly synthesized by methylmethacrylate (MMA) and methacrylisobuty polyhedral oligomeric silsesquioxane (MA-POSS) using cetylfunctional initiator of octakis(dibromoethyl) POSS (POSS-$(Br)_{16}$). Three well-defined copolymers of *s*-POSS-$PMMA_{277.3}$-b-$P(MA\text{-}POSS)_{5.8,\ 16.4,\ 25.4}$ are discussed. The introducing of P(MA-POSS) could provide the copolymer with excellent hydrophobic/oleophobic performance and thermal stability. With the increasing of MA-POSS content, although the size of core-shell micelles of *s*-POSS-$PMMA_{277.3}$-b-$P(MA\text{-}POSS)_{5.8\text{-}25.4}$ does not increased linearly due to the different self-assembly behaviors and steric effects, the surface roughness (0.44-1.41 nm) and water/hexadecane contact angles ($108^o/50^o$-$120^o/58^o$) of films, as well as the thermal stability (Td=350-380°C, Tg=112-125℃) and the storage modulus (842-1600 MPa) of copolymers are liner-increased. The effect of solvents on the self-assembled micelles and films indicates that 340-370 nm core-shell micelles, 330-370 nm sun-like stretching micelles and 180-200 nm three-layer-structured micelles are formed respectively in tetrahydrofuran (THF), chloroform($CHCl_3$) and butanone(MEK) solution. The lowest surface free energy (17.48 $m{\cdot}N{\cdot}m^{-1}$) is produced by the film casting from THF solution due to the highest surface roughness (1.12 nm) and Si content (6.01%). While, the lowest water absorption (Δm=3800ng/cm^2) and viscoelasticity ($\Delta D/\Delta f$=-0.36) film is produced by $CHCl_3$ solution, and the film casting from MEK solution obtains the highest water absorption (Δm=6500 ng/cm^2) and viscoelasticity ($\Delta D/\Delta f$=-0.15). This first example of 16-arm star-shaped POSS diblock copolymers could be used as solvent-dependent coatings.

Introduction

Polyhedral oligomeric silsesquioxane (POSS) with well-defined cube-like structures has received much attention as nanoscale building blocks to form hybrid materials. [1,2] Normally, POSS contains a silsesquioxane cage with the formula $(SiO_{1.5})n$ (n=8-14) and n organic functional groups originating at each Si atom on a cage vertex. [3,4] The functionality may therefore vary from one organic group to another [5-8] and will lead the reactive combination of POSS into polymers designed as the branch, [9,10] star-shaped, [11,12] or core-shell [13,14] structures in order to obtain hydrophobicity, or high mechanical and thermal properties. [15-18]

Actually, POSS cube can be incorporated into the polymeric system by blending,[19,20] grafting,[21,22] cross-linking[23,24] and copolymerization.[18,25,26] Up to now, the synthesis of POSS-containing polymers is mostly focused on styryl-POSS, methacrylate-POSS, norbornyl-POSS, vinyl-POSS, epoxy-POSS, phenolic-POSS, benzoxazine-POSS, amine-POSS and hydroxyl-POSS.[12,23,26-29] Shiao-Wei Kuo has reviewed the methods for synthesizing POSS compounds and have discussed how to use both mono- and multi-functional POSS monomers to develop thermoplastic and thermosetting polymers.[2] Comparatively, the multi-functional POSS is possible to form branched dendrimers, hyperbranched or star-shaped polymers, and thereby could significantly improve the properties of polymers. [9-12] In the synthesis of various POSS-based star polymers, both "grafting-to" and "grafting-from" approaches have been used as the common synthesis methods.[32] Up to now, the most arm in star-shaped POSS-containing polymer is eight-arm polymers obtained by the hydrosilylation reaction between silyl hydride-functionalized polystyrene and octavinyl POSS,[31] or by the bimolecular nonlinear polymerization utilizing either platinum-catalyzed hydrosilylation orsilanol condensation reactions. [9] or by anionic synthesis via the addition of poly(styryl)lithium to octavinyl POSS in benzene. [11] In the case of using difunctional monomers, the overall molecular structure and the number of arms are often not well-defined and polydispersity is often relatively large (PDI=1.9)[9]. Therefore, it remains a challenge to prepare uniform star polymers with molecular precision.

With the improvement of controlled polymerization techniques, multi-functional initiators for either an "arm-first" or "core-first" strategy have been developed toward this aim.[11-13] But these methods often suffer either from prolonged reaction time and incomplete reaction due to the steric hindrance of the coupling reaction in the "arm-first" strategy, or from the unequal

Department of Chemistry, School of Science, Xi'an Jiaotong University, Xi'an, China.: E-mail: heling@mail.xjtu.edu.cn; xzhao@mail.xjtu.edu.cn;

initiation efficiency and poor control over polymer chain uniformity in the "core-first" strategy. While, the controlled polymerization of ATRP is a suitable technique in obtaining the POSS block copolymers by using the multiple-arm as multi-functional initiators.[33-35] W.Yuan have reported a series of novel 8-arm star-shaped hybrid polymer (POSS-(P(MEO_2MA-*co*-OEGMA))$_8$ of P(2-(2-methoxyethoxy)ethylmethacrylate)-*co*-oligo(ethyleneglycol) methacrylate(P(MEO_2MA-*co*-OEGMA)) synthesized using octafunctional POSS-$(Cl)_8$ initiator via ATRP (PDI=1.3-1.4).[13] W.Wang used a POSS core as an initiator to polymerize methyl methacrylate for the preparation of a star-shaped POSS/PMMA-$(Cl)_8$ macroinitiator for the ATRP of styrene to obtain AB block copolymers, forming star-shaped structure with a ''core'' of POSS and an ''arms'' of polymer as PDI=1.61-1.66.[30] It can be found that the PDI for POSS-$(Cl)_8$ initiator is higher than singal initiator (PDI<1.1). This let us to consider the 16-arm initorator. As multi-initiator of ATRP for POSS-based star-shaped polymer, since both 8-arm and 16-arm are structure symmetry, it is hoped that the higher branch and grafting density in 16-arm are much more uniform and balance than 8-arm, which will led higher initiating efficiency of every active point in 16-arm initiator for ATRP and maybe a higher PDI for POSS-based star-shaped polymer than 8-arm initiator if the molecule weights are the same. However, to our best knowledge, no literature is reported on the 16-arm star-shaped diblock copolymer based on POSS obtained by ATRP techniques, and also no previous research about the properties for their self-assembled film used as the high-performance films.

Herein, this paper reports the synthesis of 16-arm star-shaped POSS-containing diblock copolymer by ATRP techniques. Octakis (dibromoethyl) polyhedral oligomeric silsesquioxanes (POSS-$(Br)_{16}$) is used as the initiator, poly (methylmethacrylate, PMMA) as the first segment, and poly (methacrylisobutyl POSS, P(MA-POSS)) as the end block. The chemical structure and the molecular weight of *s*-POSS-PMMAm-b-P(MA-POSS)n are characterized by ^{1}HNMR and SEC. The effect of both MA-POSS content and solvents on the self-assembly of *s*-POSS-PMMAm-b-P(MA-POSS)n in tetrahydrofuran (THF), chloroform ($CHCl_3$) and butanone (MEK) solutions are compared by the analysis of TEM and DLS. The surface properties of films for roughness, viscoelasticity and hydrophobicity are investigated by atomic force microscope (AFM), the quartz crystal microbalance with dissipation (QCM-D) and static contact angle (SCA). The mechanical and thermal stability of *s*-POSS-PMMAm-b-P(MA-POSS)n are obtained by TGA, DSC and DMA.

Experimental

Materials

Octakis(dibromoethyl) polyhedral oligomeric silsesquioxanes (POSS-$(Br)_{16}$, Mw=1911g·mol^{-1}) and methacrylisobutyl POSS (MA-POSS, Mw=947.3g·mol^{-1}) are purchased from Hybrid Plastics Co. (USA) and are used as received. Methyl methacrylate (MMA, 99wt%) is supplied by Aldrich, which is rinsed by 5wt% NaOH aqueous solution and ion-free water until the rinsed water reaches pH=7, followed by drying over CaH_2 for 24 h and distilling under reduced pressure to remove inhibitor before use. Toluene and tetrahydrofuran (THF) are stirred over CaH_2 for 12 h at room temperature, and distilled under reduced pressure prior to use. Cuprous chloride (CuCl) is purified according to the method of White Sides.[36] N,N,N',N',N''-pentamethyldiethylenetriamine (PMDETA, 97%) is supplied by Aldrich and is used without further purification. All other solvents are used as-received without further purification.

Preparation of *s*-POSS-PMMAm-b-P(MA-POSS)n by ATRP

When 0.4185g CuCl (4.185mmol) and a dry magnetic stirrer are added into a vacuumed Schlenk tube by N_2, the mixture of POSS-$(Br)_{16}$ (0.5g, 0.2616mmol), MMA (8.3704g, 83.70mmol), PMDETA (0.9710g, 4.185mmol) and toluene (15g) is introduced into the tube under N_2 atmosphere (Table 1). This recipe is selected for formation continuous and stable films by the enough molecular weight of PMMA and suitable MA-POSS content in the next step for final products. Reaction starts at 80℃ and keeps for 24 h in an oil bath, as shown in Scheme 1. The left catalyst is removed by passing the copolymer solution through an alumina column using THF as the solvent, and the excess solvent is removed under reduced pressure. When the colorless solution is reprecipitated into methanol and dried in a vacuum oven overnight, the white powder *s*-POSS-PMMAm is obtained. Yield: 82%.

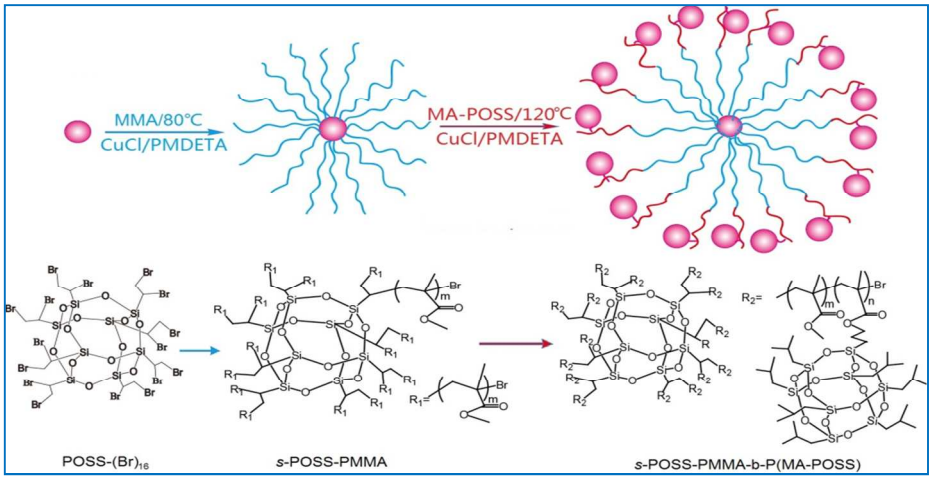

Scheme 1 Synthesis of *s*-POSS-PMMAm-b-P(MA-POSS)n

Table 1 Detailed polymerization recipes for block copolymer *s*-POSS-PMMAm-b-P(MA-POSS)n

Samples	POSS-$(Br)_{16}$/g	MMA/g	*s*-POSS-$PMMA_m$/g	MA-POSS/g	CuCl/g	PMDETA/g	Toluene/g
Sample 1	0.5	8.3704	-	-	0.4185	0.9710	15
Sample 2	-	-	0.5	0.1296	0.0137	0.02381	2
Sample 3	-	-	0.5	0.2593	0.0137	0.02381	2
Sample 4	-	-	0.5	0.5185	0.0137	0.02381	2

Table 2 Molecular weight of *s*-POSS-$PMMA_m$-b-P(MA-POSS)$_n$

Samples	Copolymers/ SEC (Theory)*	Mw(g/mol)	Mn(g/mol)	PDI(Mw/Mn)
Sample 1	*s*-POSS-$PMMA_{277.3(320)}$	29230	23190	1.261
Sample 2	*s*-POSS-$PMMA_{277.3}$-b-P(MA-POSS)$_{5.8(8)}$	34690	24990	1.388
Sample 3	*s*-POSS-$PMMA_{277.3}$-b-P(MA-POSS)$_{16.5(16)}$	44840	34450	1.302
Sample 4	*s*-POSS-$PMMA_{277.3}$-b- P(MA-POSS)$_{25.4(32)}$	53310	37910	1.406

When *s*-POSS-PMMAm is dissolved in toluene in a schlenk tube, a mixture of MA-POSS, CuCl and PMDETA is charged under N_2 atmosphere. Then, the reaction is permitted to last for 24 h at 110℃ in an oil bath as Scheme 1. The left catalyst and the excess solvent are removed by the same way as above. The resulting star-shaped copolymer *s*-POSS-$PMMA_m$-b-P(MA-POSS)$_n$ (Sample 2-4) are obtained in a yield of 73-78%. The detailed polymerization recipes are listed in Table 1.

The films of *s*-POSS-$PMMA_m$-b-P(MA-POSS)$_n$ are prepared by casting the solutions onto a glass substrate and then drying it at ambient temperature.

Characterization

The proton nuclear magnetic resonance (^{1}H-NMR) measurement is performed on a Bruker AV-500 spectrometer using $CDCCl_3$ as solvent and tetramethylsilane (TMS) as the internal reference. The molecular weight of samples are determined on a DAWN EOS size exclusion chromatography (SEC) (Wyatt Technology, USA). The eluent of THF (containing 0.01 mol·L^{-1} LiCl at 25℃) is used at a flow rate of 0.5 mL·min^{-1}. The molecular weight is calibrated by the polystyrene standards.

Transmission electron microscopy (TEM) is used to understand the morphology of self-assembled *s*-POSS-PMMAm-b-P(MA-POSS)n in THF, $CHCl_3$ and MEK solutions. The measurements are conducted by a JEM-3010 in an acceleration voltage of 100 kV. Samples are prepared by drop-casting micelle solutions onto carbon-coated copper grids, and then air-drying at room temperature before measurement. Dynamic light scattering (DLS) analysis is used to obtain the aggregates of samples in THF, $CHCl_3$ and MEK solutions (0.01 g·mL^{-1} sample solutions) by using a MALVERN Nano ZS 90 (Malvern Instruments, U.K.) equipped with a He-Ne laser (λ=632.8 nm). The scattering data are recorded at 25±0.1°C in back-scattering modus at a scattering angle of 2θ=173°.

Atomic force microscope (AFM) for characterizing the surface topographies and roughness of the obtained film is performed by NT-MDT new Solver-Next under 38-42% R.H. Tip information: radius <10 nm, cantilever length 90±5 mm; width 40 ±3 mm; thickness 2.0±0.5 mm, resonant frequency 330 kHz, force constant 48 N·m^{-1}. X-Ray photoelectron spectroscopy (XPS) measurement is processed on the air-exposed film surface by an AXIS ULTRA (England, KRATOS ANALYTICAL Ltd) using an Al mono Kα X-ray source (1486.6 eV) operated at 150 W. The overview scans are obtained with pass energy of 160 eV and acquisition times of 220s. Static contact angles (SCAs) measurement for deionized water and hexadecane on the air-exposed surfaces of the films are conducted on a JY-82 contact angle goniometer (Testing Machine Co. Ltd. China) by the sessile drop method with a microsyringe at 25℃. The surface free energy is calculated by using the water contact angles.[37]

Q-Sense E1 Quartz crystal microbalance with dissipation monitoring (QCM-D, Sweden) for water adsorption of film surfaces is measured at 25℃ by AT-cut piezoelectric quartz crystals covered with gold with a fundamental frequency of 5 MHz and a diameter of 14 mm. The films are prepared by dropping 0.2 μL copolymer solutions (1wt%) on the surfaces of quartz crystals and drying in a vacuum oven at 30℃ for 12 h. The Δf and ΔD are recorded at 15 MHz with air as the baseline. Δm is calculated by $\Delta m=K\Delta f$[38] according to K=-5.9ng/Hz cm^2.[39]

Thermogravimetry (TGA) is performed under N_2 atmosphere with 10ºC/min temperature rise at 700ºC using TGA analyzer (STA449C Jupiter from NETZSCH). Differential Scanning Calorimeter (DSC) thermo-scans of samples are recorded using a NETZCH DSC-200 apparatus. To eliminate thermal history, all data are collected during a second heating run at a scanning rate of 10℃·min^{-1} from -50℃ to 200℃ under a dry nitrogen atmosphere, after heating the sample from 20℃ to 100 ℃ at 10℃ min^{-1} and then rapidly cooling to -50℃ using liquid nitrogen. Dynamic mechanical analysis (DMA) is carried out by using a DMA Q800 instrument with tension mode. The sample films are cut into 12 mm×8 mm×0.0200 mm (lengh×wide×thick), and then are equilibrated for 5 min at 20℃, heated to 200℃ at constant heating rate of 5℃/min under nitrogen and frequency of 1 Hz.

3. Results and Discussion

3.1 Synthesis of *s*-POSS-PMMAm-b-P(MA-POSS)n

The star-shaped diblock copolymers *s*-POSS-PMMAm-b-P(MA-POSS)n are synthesized via ATRP using an POSS-$(Br)_{16}$ nanocage to initiate MMA and MA-POSS. ^{1}H-NMR spectrum for

both *s*-POSS-PMMA and *s*-POSS-PMMAm-b-P(MA-POSS)n is shown in Fig.1. Compared with δ_H of POSS-$(Br)_{16}$ (Fig.1a) at 3.65ppm (b) for Si-CH-, 3.8 and 4.05ppm (a^2 and a^1) for -CH_2-, the chemical structure of *s*-POSS-PMMAm (Fig.1b) is realized by δ_H (ppm) at 3.60 (a) for -OCH_3 in PMMA, 1.86 (b) for Si-CH- in POSS, 0.85 (c) for -CH_3 in PMMA and 1.56 (d) for -CH_2- in PMMA. The typical δ_H of *s*-POSS-PMMAm-b-P(MA-POSS)n (Fig.1c) at 3.82ppm (a) for -O-CH_2- in P(MA-POSS) and at 3.60ppm (b) for -OCH_3 in PMMA, together with disappearing δ_H at 5.5ppm and 6.2ppm (a) for =CH_2 in MA-POSS (Fig.1d), has confirmed the diblock structure of *s*-POSS-PMMA-b-P(MA-POSS) as designed.

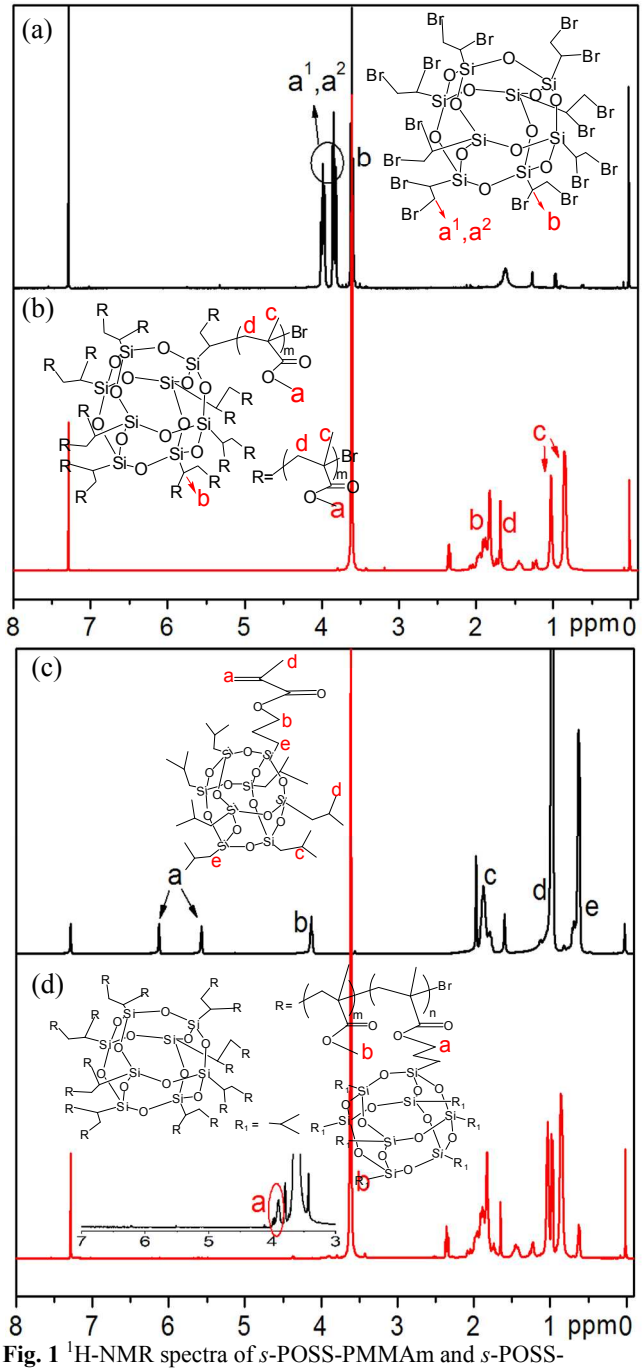

Fig. 1 ^{1}H-NMR spectra of *s*-POSS-PMMAm and *s*-POSS-$PMMA_m$-b-P(MA-POSS)$_n$

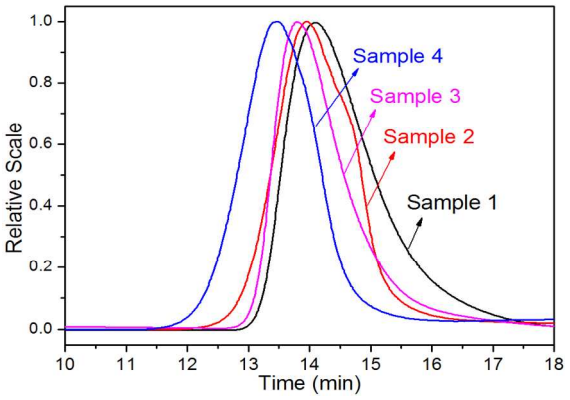

Fig. 2 SEC curves of *s*-POSS-$PMMA_m$-b-P(MA-POSS)$_n$

Furthermore, the molecular weight (Mw) is determined by SEC plot in Fig.2 and Table 2. Mw as 29230 g·mol^{-1} for Sample 1 (*s*-POSS-PMMAm), 34690, 44840 and 53310 g·mol^{-1} for Sample 2-4 (*s*-POSS-PMMAmb-P(MA-POSS)n) with the corresponding molecular weight distribution (PDI) of 1.261, 1.388, 1.302 and 1.406, respectively, have indicated the typical ATRP polymerization. Compared with 8-arm star-shaped hybrid with a "core" of POSS and an "arms" of polymer obtained by POSS-$(Cl)_8$ initiator via ATRP as PDI=1.3-1.4[13] and PDI=1.61-1.66,[30] these PDI (1.261-1.406) from POSS-$(Br)_{16}$ initiator for star-shaped hybrid in this paper is not higher than POSS-$(Cl)_8$ initiator. This suggest that 16-arm POSS-cored star-shaped hybrid with higher branch are able to obtain a uniform grafting density copolymer in ATRP approach. Therefore, the degree of *m* in Sample 1 of *s*-POSS-$PMMA_m$ is evaluated as 277.3 (the theory *m* is 320 by calculation), and the degree of *n* in Sample 2-4 of *s*-POSS-$PMMA_{277.3}$-b-P(MA-POSS)$_n$ are evaluated as 5.8, 16.4, 25.4 (the theory *n* is 8, 16, 32, calculated by the adding ratio of monomers and the initiators). These results could suggest that the average number of P(MA-POSS) arms attached to one *s*-POSS-b-PMMA nanocage is 5.8, 16.4 and 25.4 in Sample 2-4.

3.2 The micelles and film surface self-assembled by *s*-POSS-$PMMA_{277.3}$-b-P(MA-POSS)$_{5.8\text{-}25.4}$

Considering different solubility of POSS, PMMA and P(MA-POSS) segments in THF solution, the self-assembly of Sample 1-4 with different content of P(MA-POSS) is investigated in Fig.3. Sample 1 of *s*-POSS-PMMA (Fig.3a) shows 150-200 nm core/shell micelles, which is corresponded to 136.3 nm aggregates in DLS curve (with a little of 7.1 nm unimers) (Fig.3e). The micelles are formed by POSS core (the black region in the centre) and PMMA shell (the light region in the edge) due to much better solubility of PMMA than POSS, which is explained in the enlarged pattern and schematic diagram (Fig.3a).

However, with the introduction of MA-POSS and increasing of MA-POSS content (15.7%-45.2wt%), the size of self-assembled core/shell micelles does not increased linearly. For Sample 2 of *s*-POSS-$PMMA_{277.3}$-b-P(MA-POSS)$_{5.8}$, since only 5.8/16 branches are successful occupied by P(MA-POSS) segments, the less solubility of P(MA-POSS) segment and POSS-$(Br)_{16}$ initiator are aggregated into the inner core (dark region), and the better solubility of PMMA segment occupied by P(MA-POSS) is also pulled back into the core, but other unoccupied

PMMA segment is stretching outside (the whitish region) as shown in the scheme (Fig.3b), therefore, 140-170 nm core/shell micelles are formed as the similar size of 172.6 nm (82%) in DLS curve (Fig.3e). This indicates that the introduction of P(MA-POSS) segment into the copolymer is not accordingly increased the size of micelles. While, for Sample 3 of *s*-POSS-PMMA$_{277.3}$-b-P(MA-POSS)$_{16.5}$, 340-360 nm core/shell micelles are formed with 40 nm compact shell (Fig.3c), which are further confirmed by 311.3nm aggregates in DLS curve (Fig.3e). Since the arms are occupied as 16.5/16 (almost all the occupied PMMA arms have been hold by P(MA-POSS)), the inner core is formed by much content of P(MA-POSS) together with POSS-(Br)$_{16}$ so that the bigger core is produced like the scheme in Fig.3c to increase the size of micelles. For Sample 4 of *s*-POSS-PMMA$_{277.3}$-b-P(MA-POSS)$_{25.4}$ with much content of MA-POSS (25.4/16) in Fig.3d, 200-220 nm micelles with inlayed-dark-spot morphology are confirmed as 227.0 nm by DLS curve in Fig.3e. Since the flexibility copolymer and the movement of *s*-POSS-PMMA$_{277.3}$-b-P(MA-POSS)$_{25.4}$ are restricted by the heavy P(MA-POSS)$_{25.4}$, the smaller aggregates in Sample 4 are quickly gathered to limit the formation of larger aggregates. Thus, the size of micelles is smaller than that of Sample 3.

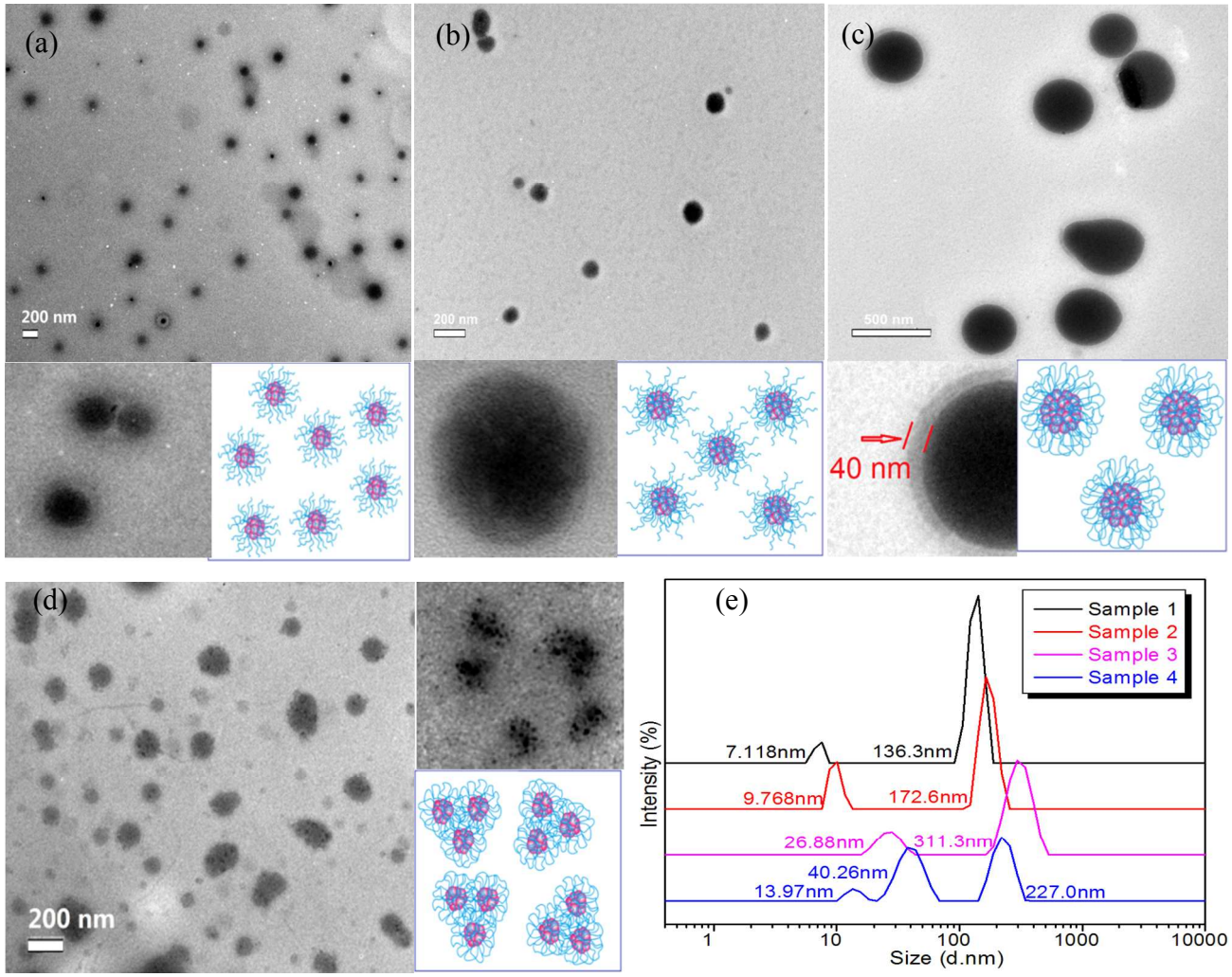

Fig. 3 TEM morphology of micelles for Sample 1-4 (a-d) in THF solution and the corresponding DLS curves (e)

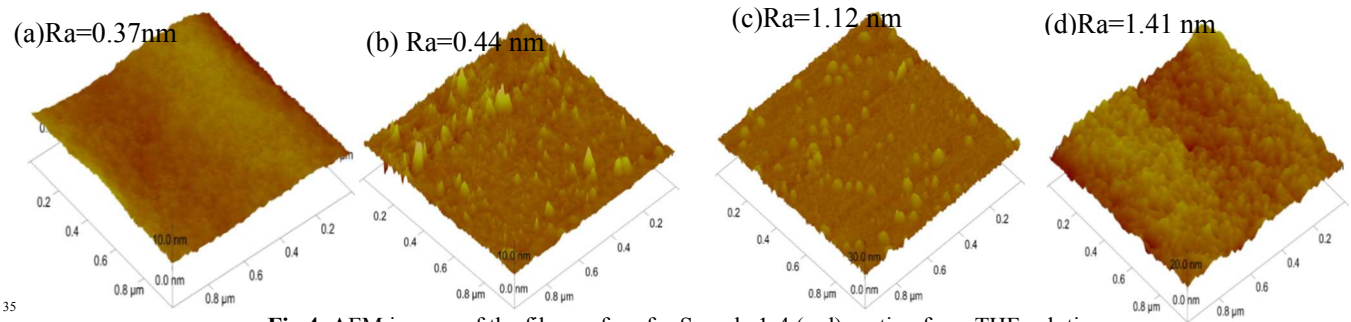

Fig.4 AFM images of the film surface for Sample 1-4 (a-d) casting from THF solution

Table 3 The micelles and the properties of film surface

Samples	Sample 1	Sample 2	Sample 3	Sample 4	Sample 3	Sample 3
Solvent	THF	THF	THF	THF	$CHCl_3$	MEK
Micelle/nm (TEM)	150-200	140-170	340-360	200-220	330-370	180-220
Morphology (TEM)	core/shell	core/shell	core/shell	multi-core /shell	sun-like stretching	core/multi-shell
Micelle/nm (DLS)	136.3/7.1*	172.6/9.7	311.3/26.88	227.0/40.26	407.2/11.7	206.5/8.44
Roughness/nm (Ra)	0.37	0.44	1.12	1.41	0.291	0.57
Rough curve/nm	-0.6 ~ 0.6	-0.7 ~ 0.9	-2.0 ~ 3.4	-2.2 ~ 3.5	-0.6 ~ 0.8	-0.1 ~ 1.2
SCAs/° (Water/Hex)	112/28	108/50	114/54	120/58	104/22	100/20
γ/mNm^{-1}	24.46	19.11	17.48	16.16	25.94	26.74
Δm ng/cm^2	7900	-	4600	-	3800	6500
$\Delta D/\Delta f$	-0.075	-	-0.19	-	-0.36	-0.15

Where, * stands for the unimers.

These self-assemble results reveal that Sample 2-4 of *s*-POSS-PMMA$_{277.3}$-b-P(MA-POSS)$_{5.8\text{-}25.4}$ are mainly self-assembled as POSS/P(MA-POSS) core and PMMA shell due to less solubility of inorganic POSS/P(MA-POSS) core and better solubility of PMMA segments in THF solution. These results are similar to 8-arm star-shaped POSS-containing copolymer, as previous reported by W.Yuan.[13] Theie results show that POSS-(P(MEO$_2$MA-co-OEGMA))$_8$ with an inorganic POSS core and eight organic P(MEO$_2$MA-co-OEGMA) arms can assemble into micelles in water as the hydrophilic P(MEO$_2$MA-*co*-OEGMA) arms mainly in the shell of the micelles and the hydrophobic POSS cores mainly in the core of the micelles. Therefore, it is possible to suggest that the self-assembly behavior of different arms POSS-containing polymer are similar, even they are in different grafting density.

The effect of these self-assembled micelles on the surface morphology of casted films is characterized by AFM in Fig.4. Sample 1 displays a rather smooth surface (Fig.4a, Ra=0.367 nm) with the rough curve float between -0.6 nm and 0.6 nm (Table 3). However, Sample 2-4 show ordered convexes and heaves on the film surface with Ra=0.438 nm, 1.12 nm and 1.41nm for surface roughness, respectively (Fig.4 b-d). This is because P(MA-POSS) segment tends to migrate onto the film surface to form the convexes in increasing the roughness, which has been proved by literature.[40] Therefore, SCAs and the surface free energies calculated in Table 3 indicate that the films of Sample 1-4 show the obvious hydrophobicity (108-120° water contact angles), enough oleophobicity (28-58° hexadecane contact angles) and lower surface free energy (16.16-24.46mN/m), and SCAs is increased with the increasing of MA-POSS content due to the improving in surface roughness.

3.3 Thermal/mechanical properties of *s*-POSS-PMMA$_{277.3}$-b-P(MA-POSS)$_{5.8\text{-}25.4}$

The thermal stability of *s*-POSS-PMMA$_{277.3}$-b-P(MA-POSS)$_{5.8\text{-}25.4}$ is investigated by TGA at the thermal degradability ranging from 25℃ to 800℃ (Fig.5). POSS-(Br)$_{16}$ and *s*-POSS-PMMA are used for comparison. POSS-(Br)$_{16}$ presents two degradations at 300℃-400℃ and 400°C-550℃ (Fig.5a), which results from -CHBr-CH$_2$Br (with 45wt% weight loss) and the skeleton of Si-O-

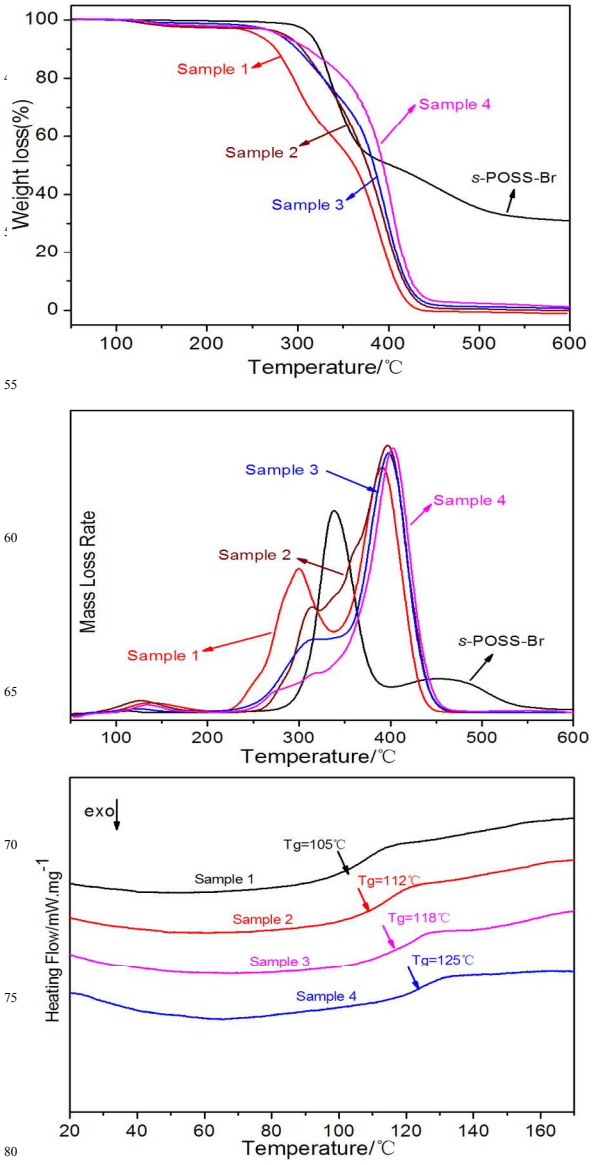

Fig.5 TGA curves (a), DTG (b) and DSC thermograms (c) of Sample 1- 4

Si (with 27wt% weight loss). However, the first degradation temperature for Sample 1-4 occurs at 235°C (Sample 1), 250°C (Sample 2), 255°C (Sample 3) and 270°C (Sample 4), respectively, due to the thermal degradability of side chains of PMMA, and the second one occurs at 350°C, 365°C, 375°C and 380°C accordingly due to the backbone of P(MA-POSS) and the skeleton of Si-O-Si. The final remainders are increased with the increasing of MA-POSS content. Therefore, MA-POSS could improve the thermal degradability obviously. On the other hand, the thermal degradability curves of samples 1-4 are also confirmed by the mass loss rate in DTG curves in Fig.5b. Sample 1 presents separated two peaks happened at 300°C and 400°C, but these two peaks tend to blend into one peak in Sample 2-4 because of better compatibility of P(MA-POSS) and PMMA (Fig.5b). In addition, DSC measurement in Fig.5c also indicates that the glass transition temperatures (T_g) for Sample 1-4 are located at 105℃, 112℃, 118℃ and 125℃, respectively. These results not only confirm the successful synthesis of *s*-POSS-PMMA-b-P(MA-POSS) copolymer, but also prove that the compatibility becomes better with MA-POSS increasing.

Furthermore, the dynamic mechanical properties of Sample 1-4 are studied by DMA for the storage modulus (Fig.6a) and for the loss factor (Fig.6b). With the increasing of MA-POSS content, the storage modulus of samples is increased obviously from 842 MPa for Sample 1 to 1160, 1420 and 1600 MPa for Sample 2-4 (Fig.6a), showing that MA-POSS could limit the movement of the segments and improve the storage modulus. Meanwhile, the starting softening temperature of Sample 1-4 in Fig.6b is also increased at 104℃, 109℃, 115℃ and 125℃ with the increasing of MA-POSS content, and the loss factor is highly consistent with the Tg values in DSC curves (Fig 5c).

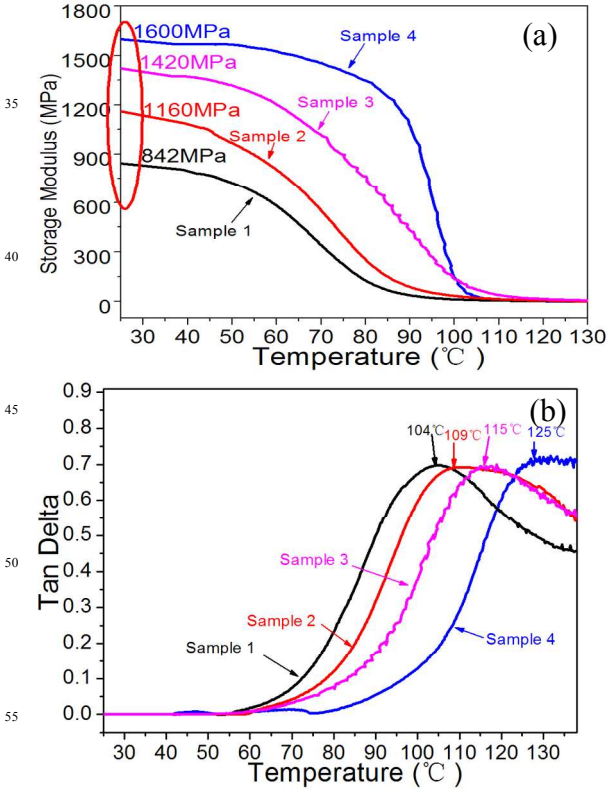

Fig. 6 Storage modulus (a) and Tan delta of mechanical tensile stress (b) for the films

3.4 The effect of solvents on micelles and film surface

In order to understand the effect of solvents on the self-assembled micelles of copolymers, THF, $CHCl_3$ and MEK are selected based on that MEK has the best solubility but $CHCl_3$ has the worst one. Sample 3 of *s*-POSS-PMMA$_{277.3}$-b-P(MA-POSS)$_{16.5}$ is selected as the discussed example, based on the results of self-assembled micelles and the films through comparative discussion above for Sample 2-4. Compared with 360 nm core-shell micelles in THF solution discussed above (Fig.3c), Sample 3 forms 330-370 nm sun-like stretching micelles in $CHCl_3$ solution (Fig.7a), which is a little smaller than 407.2 nm in DLS curve due to PMMA stretching shell caused by its better solubility (Fig.7c). But in MEK solution (Fig.7b), Sample 3 shows 200 nm three-layer-structured micelles as black core, dark shell and black crown, which are correspond to 206.5nm micelles in DLS curve (Fig.7c). The core and the crown are formed by P(MA-POSS) segment, and the shell is formed by PMMA segment.

Comparing with the micelles in THF (Fig.3c, 360 nm core-shell micelles), $CHCl_3$ (Fig.7a, 330-370 nm sun-like stretching micelles) and MEK (Fig.7b, 200 nm three-layer-structured micelles) solutions, the different morphology is attributed to the solubility, the flexibility and the movement of different segments. In THF and $CHCl_3$, the better solubility, flexibility and movement of PMMA segments are intertwined tightly into shell, but P(MA-POSS) segments are gathered into the inner core. While, in MEK, since the heavy P(MA-POSS) segments are easy to aggregate but POSS initiator dose not move easily into the inner core due to the space effects, thus three-layer-structured micelles are formed as scheme in Fig.7b.

Although XPS analysis for Sample 3 reveals that P(MA-POSS) segments in three solvents of THF, $CHCl_3$ and MEK are all easily migrate onto the film surface, due to higher Si content on the film surface (4.62%-6.01%) than the powder (2.75%) (Fig.7d), THF solution is the best solvent for migration of P(MA-POSS) segments to obtain a higher Si content surface (6.01%) than the films casting from $CHCl_3$ and MEK (4.83% and 4.62%). In fact, this strong migration will result in the increasing of surface roughness of film. Therefore, compared with convexes/heaves surface with 30 nm roughness casting from THF solution (Fig.4c, Ra=1.12 nm), the film casting from $CHCl_3$ and MEK solutions present rather smooth surface as 5 nm roughness in Fig.7e (Ra=0.29nm) and Fig.7f (Ra=0.57 nm).

For the surface wettability of these films, Table 3 shows that the film casting from THF solution has higher water/hexadecane contact angles (114°/54°) and lower surface free energy (17.48 mN/m) than the film casting from $CHCl_3$ (104°/22°, 25.94mN/m) and MEK (100°/20°, 26.74mN/m) solutions. This is not only because 1.12 nm Ra casting from THF solution (Fig.4c) is much higher than casting from $CHCl_3$ and from MEK, but also because the THF film has much higher Si content (6.01%) than other two films (4.83% and 4.62%). This is corresponding to the results that increasing of P(MA-POSS) segment tends to form higher roughness owing to the migrating of P(MA-POSS) onto the film surface for Sample 2-4 (Table 3). Therefore, although the roughness of film casting from MEK (0.57nm) is higher than that from $CHCl_3$ (0.29nm), the Si content on the film surface casting $CHCl_3$ (4.83%) is higher than MEK (4.62%), the SCA value of $CHCl_3$-casting film is higher than MEK-casting film. These

results suggest that the higher roughness and higher Si content on the film surface contribute much to the higher contact angles.

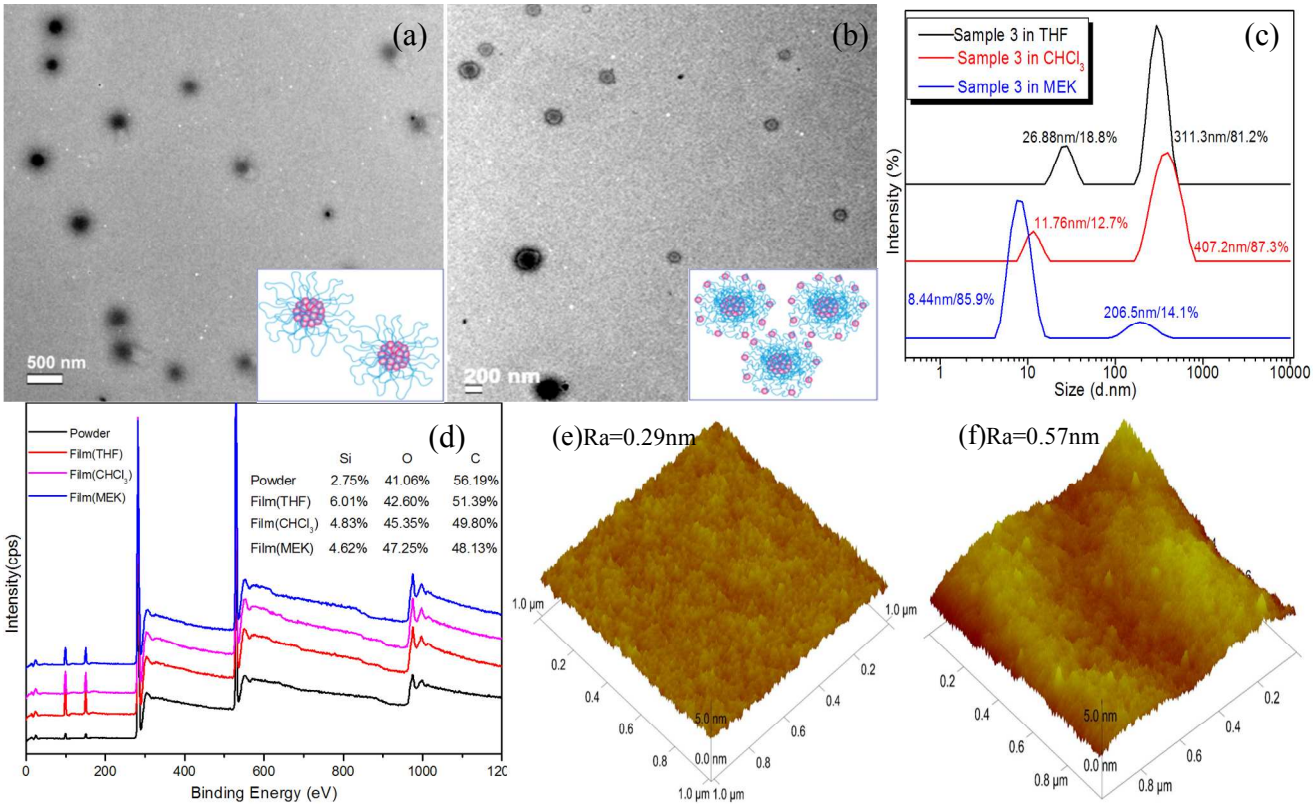

Fig.7 TEM morphology of micelles in $CHCl_3$(a), MEK(b) and the corresponding DLS curves (c), the chemical composition of films by XPS (d), and AFM images of the film surface casting from $CHCl_3$(e) and MEK(f) solutions for Sample 3

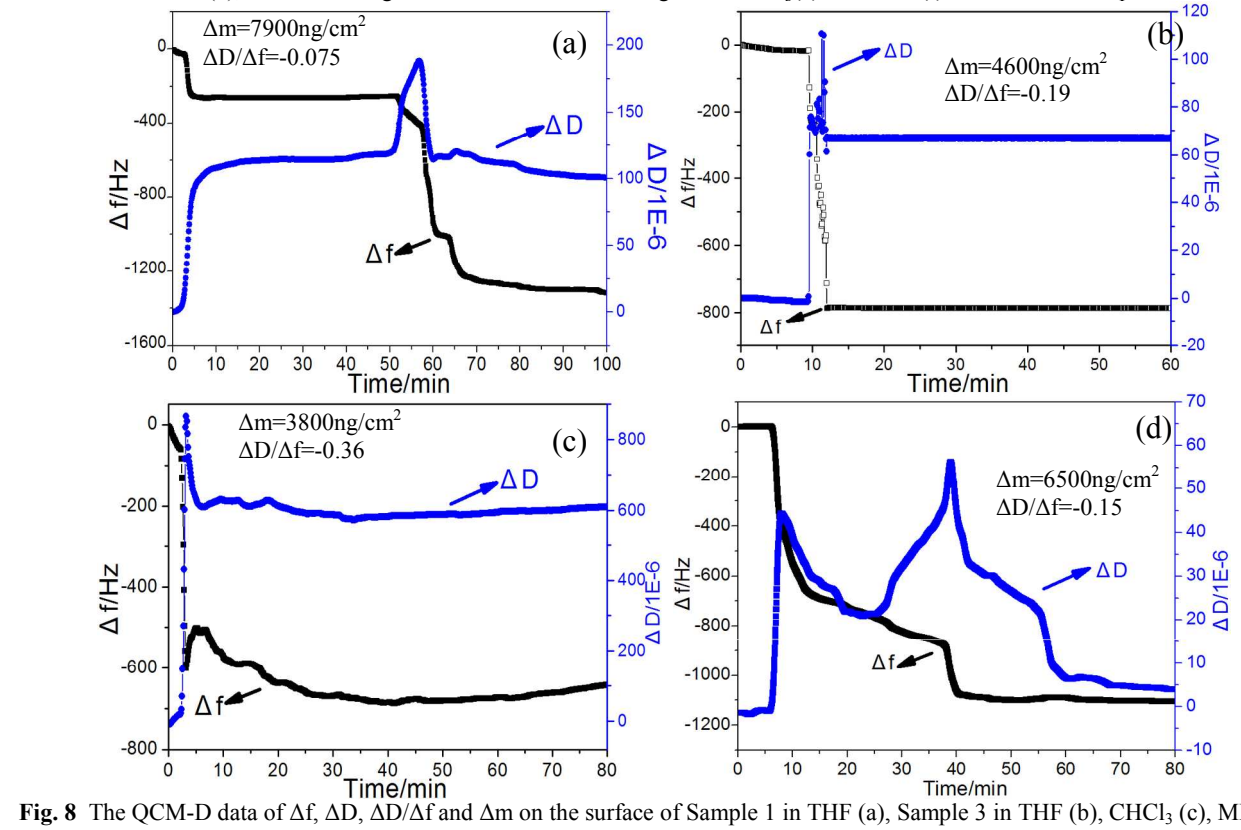

Fig. 8 The QCM-D data of Δf, ΔD, ΔD/Δf and Δm on the surface of Sample 1 in THF (a), Sample 3 in THF (b), $CHCl_3$ (c), MEK (d) solution

3.6 The surface water adsorption of films

The surface water adsorption of films (Sample 3) is evaluated by QCM-D measurement in Fig.8. The Δf in the adsorption curves is used to indicate the adsorbed amounts of probe liquids, ΔD/Δf at the end of water absorption is used to indicate the viscoelasticity of the adsorbed layer (the higher $\Delta D/\Delta f$ value indicating the softer adsorbed layer) and Δm calculated is used to express the adsorption amount. The QCM-D result for Sample 1 (*s*-POSS-PMMA, THF) is used for comparison. There are two equilibrium processes of Δf and ΔD for *s*-POSS-PMMA film in Fig.8a. 5-50 minutes process shows that the film could give the obvious resistance to water adsorption as the stable structure. However, the process of Δf decreasing and ΔD increasing at 50-65 minutes tells that the structure of film has collapsed and reconstructed to reach another equilibrium until 65 minute. For Sample 3 casting from THF solution in Fig.8b, with the water absorption after the air equilibrium, a seeking balance process of the water adsorption and the viscoelasticity of the adsorbed layer is found at 9-12 minute by a dynamic changing process of ΔD increasing with Δ*f* decreasing until to keep an exceeding equilibrium process due to the stable structure formed. The amount of water absorption in Sample 3 (Δm=4600ng/cm^2) and the viscoelasticity (ΔD/Δf=-0.19) is much lower than Sample 1 (Δm=7900ng/cm^2, ΔD/Δf=-0.075), which proves that the introduction of P(MA-POSS) into the copolymer in Sample 3 could give the film obvious resistance to water adsorption and to keep a stable film than Sample 1 after water absorption. For the film casting from $CHCl_3$ solution (Sample 3, Fig.8c), the water adsorption and the viscoelasticity of the adsorbed layer reach equilibrium at 30 minute with Δm=3800ng/cm^2 and ΔD/Δf=-0.36, showing the least water adsorption and the lowest viscoelasticity. In Fig.8d for the film casting from MEK solution (Sample 3), a dynamic seeking balance process occurs at 8-60 minute with the water adsorption increasing along the decreasing of Δf. The water adsorption (Δm=6500ng/cm^2) and the viscoelasticity (ΔD/Δf=-0.15) of the adsorbed layer is higher than the film casting from $CHCl_3$ (Δm=3800ng/cm^2 and ΔD/Δf=-0.36), but lower than the film casting from THF solution (Δm=4600ng/cm^2, ΔD/Δf=-0.19). Comparatively, the times of film to reach equilibrium after absorption water are 12 minutes, 30 minutes and 60 minutes respectively. The film casting from $CHCl_3$ solution gives the lowest water adsorption and lowest wettability state (Δm=3800ng/cm^2 and ΔD/Δf=-0.36), but a less stability of the film after water absorption. Whereas the film casting from MEK solution is the worst one for the most water adsorption (Δm=6500ng/cm^2) and viscoelasticity (ΔD/Δf=-0.15).

4. Conclusions

Star-shaped POSS diblock copolymers of *s*-POSS-PMMA$_{277.3}$-b-P(MA-POSS)$_{5.8,\ 16.4,\ 25.4}$ are synthesized by using 16-arm POSS (POSS-(Br)$_{16}$) to initiate MMA and P(MA-POSS). The effect of MA-POSS content and the solvents on the properties of star-shaped diblock copolymers and the self-assembled films is conducted. MA-POSS could improve obviously the surface roughness and the water/hexadecane contact angles of films, and the thermal stability and the storage modulus of copolymers. This 16-arm star-shaped POSS diblock copolymer could be used as a solvent-dependent coating material based on the properties from the effect of solvents on the self-assembled films. Since different micelles are formed in THF, $CHCl_3$ and MEK solutions, different surface properties are obtained as: THF could produce the film with highest surface roughness and Si content, and therefore the lowest surface free energy, $CHCl_3$ could give the film with the lowest water absorption and viscoelasticity, but MEK enable to produce the highest water absorption and viscoelasticity film.

Acknowledgements

This work has been financially supported by the National Basic Research Program of China (973 Program, No.2012CB720904), by the National Natural Science Foundation of China (NSFC Grants 51373133, 51073126, 21171138), by the State Administration of Cultural Heritage (20110128) and by the Specialized Research Fund for the Doctoral Program of Higher Education of China (SRFDP No. 20130201110033). The authors also wish to express their gratitude for the MOE Key Laboratory for Non-equilibrium Condensed Matter and Quantum Engineering of Xi'an Jiaotong University.

Notes and references

1. D. B. Cordes, P. D. Lickiss and F. Rataboul, *Chem. Rev.*, 2010, 110, 2081-2173.
2. S. W, Kuo and F. C. Chang, Prog. Polym. Sci., 2011, 36, 1649-1696.
3. A. J. Guenthner, K. R. Lamison, L. M. Lubin, T. S. Haddad and J. M. Mabry, *Ind. Eng. Chem. Res.,* 2012, 51, 12282-12293.
4. M. F. Roll, J. W. Kampf, Y. Kim, E. Yi and R. M. Laine, J. Am. Chem. Soc., 2010, 132, 10171-10183
5. F. K. Wang, X. Lu and C. He, *J. Mater. Chem.*, 2011, 21, 2775-2782.
6. W. Zhang, J. Yuan, S. Weiss, X. Ye, C. Li and A. H. E. Meuller, *Macromolecules,* 2011, 44, 6891-6898.
7. V. A.Ganesh, A. S. Nair, H. K. Raut, T. T. Y.Tan, C. He, S. Ramakrishna and J. Xu, *J. Mater. Chem.*, 2012, 22, 18479-18485.
8. Y. Li, X. H. Dong, K. Guo, Z. Wang, Z. Chen, C. Wesdemiotis, R. P. Quirk, W. B. Zhang and S. Z. D. Cheng, *ACS Macro Lett.,* 2012, 1, 834-839.
9. N. Xu, E. J. Stark, P. R. Dvornic, D. J. Meier, J. Hu and C. Hartmann-Thompson, *Macromolecules,* 2012, 45, 4730-4739.
10. B. Yu, X. Jiang and J. Yin, *Macromolecules,* 2012, 45, 7135-7142.
11. W. B. Zhang, J. He, K. Yue, C. Liu, P. Ni, R. P. Quirk and S. Z. D. Cheng, *Macromolecules,* 2012, 45, 8571-8579.
12. B. H. Tan, H. Hussain, T. T. Lin, Y. C. Chua, Y. W. Leong, W. W. Tjiu, P. K. Wong and C. B. He, *Langmuir,* 2011, 27, 10538-10547.
13. W. Yuan, T. Shen, X. Liu, J. Ren, Mater. Lett., 2013,111, 9-12.
14. F. Du, J. Tian, H. Wang, B. Liu, B. Jin and R. Bai, *Macromolecules*, 2012, 45, 3086-3093.
15. V. A. Ganesh, A. S. Nair, H. K. Raut, T. T. Y. Tan, C. He, S. Ramakrishna and J. Xu, *J. Mater. Chem.*, 2012, 22, 18479-18485.
16. A. KOTAL, S. SI, T. K. PAIRA, T. K. MANDAL, J. Polym. Sci. Part A: Polym. Chem., 2008 46, 1111-1123.
17 M. Grala, Z. Bartczak and M. Pracella, Polym. Composites, 2013, 929-941.
18. S. M. Ramirez, Y. J. Diaz, C. M. Sahagun, M. W. Duff, O. B. Lawal, S. T. Iacono and J. M. Mabry, *Polym. Chem.*, 2013, 4, 2230-2234.
19. P. Chen, X. Huang, Q. Zhang, K. Xi and X. Jia, *Polymer,* 2013, 54, 1091-1097.
20. O. Monticelli, A. Fina, A. Ullah, and P. Waghmare, *Macromolecules*, 2009, 42, 6614-6623.
21. O. Monticelli, A. Fina, E. S. Cozza, M. Pratoc and V. Bruzzo, *J. Mater. Chem.*, 2011, 21, 18049-18054.
22. A, Fina, D, Tabuani, T, Peijs and G, Camino, *Polymer*, 2009, 50, 218-226.
23. F. Alves, P. Scholder and I. Nischang, *ACS Appl. Mater. Interfaces*, 2013, 5, 2517-2526.

24. D. Chen, J. Nie, S. Yi, W. Wu, Y. Zhong, J. Liao, C. Huang, Polym. Degrad. Stab., 2010, 95, 618-626.
25. Y. C. Lin and S. W. Kuo, *Polym. Chem.*, 2012, 3, 882-891.
26. S. K. Kim, D. G. Kim, A. Lee, H. S. Sohn, J. J. Wie, N. A. Nguyen, M. E. Mackay and J. C. Lee, *Macromolecules*, 2012, 45, 9347-9356.
27. M. E. Wright, B. J. Petteys, A. J. Guenthner, S. Fallis, G. R. Yandek, S. J. Tomczak, T. K. Minton and A. Brunsvold, *Macromolecules,* 2006, 39*,* 4710-4718.
28. C. Zhang, S. Guang, X. Zhu, H. Xu, X. Liu and M. Jiang, *J. Phys. Chem. C,* 2010, 114*,* 22455-22461.
29. M. J. Abad, L. Barral, D. P. Fasce and R. J. J. Williams, *Macromolecules,* 2003, 36*,* 3128-3135.
30. W. Wang, M. Fei, X. Jie, P. Wang, H. Cao and J. Yu, *Polym. Bull.*, 2010, 65, 863-872.
31. X. Yu, S. Zhong, X. Li, Y. Tu, S. Yang, R. M. V. Horn, C. Ni, D. J. Pochan, R. P. Quirk, C. Wesdemiotis, W. B. Zhang and S. Z. D. Cheng, J. Am. Chem. Soc., 2010, 132, 16741-16744.
32. D. G. Kim, H. Kang, S. Han and J. C. Lee, *ACS Appl. Mater. Interfaces*, 2012, 4, 5898-5906.
33. J. Pyun and K. Matyjaszewski, *Macromolecules*, 2000, 33*,* 217-220.
34. W. Zhang and A. H. E. Müller, Prog. Polym. Sci., 2013, 38, 1121-1162.
35. H. Hussain, B. H. Tan, G. L. Seah, Y. Liu, C. B. He and T. P. Davis, *Langmuir*, 2010, 26(14), 11763-11773.
36. G, M. Whitesides, J, S. Sadowski and J. Lilburn, *J. Am. Chem. Soc.*, 1974, 96, 2829-2835.
37. S. Saïdi, F. Guittard, C. Guimon and S. Géribaldi, Eur. Polym. J., 2006, 42, 702-710.
38. S. G. Verwendung von Schwingquarzen zur Wagung dunner Schichten und zur Mikrowagung. *Z Phys,* 1959, 155, 206-222.
39. B. Peng, X. Chu, Y. Li, D. Li, Y. Chen and J. Zhao, *Polymer*, 2013, 54, 5779-5789.
40. K. Y. Mya, E. M. J. Lin, C. S. Gudipati, L. Shen and C. He, *J. Phys. Chem. B,* 2010, 114, 9119-9127.

A table of contents entry.

Color Graphic

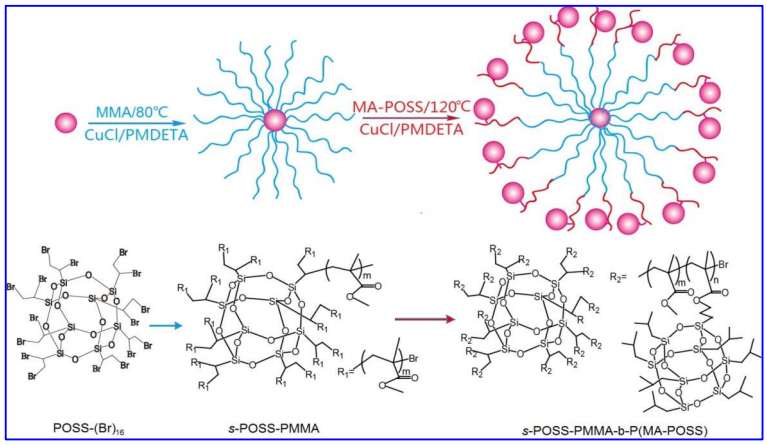

Text:

This first example of 16-arm star-shaped diblock copolymers *s*-POSS-PMMA$_{277.3}$-b-P(MA-POSS)$_{5.8,\ 16.4,\ 25.4}$ could be used as solvent-dependent coatings.